

Inducing and exploiting vulnerabilities for the treatment of liver cancer

Cun Wang^{1,2,7}, Serena Vegna^{3,7}, Haojie Jin^{1,2,7}, Bente Benedict^{3,7}, Cor Lieftink², Christel Ramirez³, Rodrigo Leite de Oliveira², Ben Morris², Jules Gadiot³, Wei Wang⁴, Aimée du Chatinier², Liqin Wang², Dongmei Gao⁵, Bastiaan Evers², Guangzhi Jin⁶, Zheng Xue², Arnout Schepers², Fleur Jochems², Antonio Mulero Sanchez², Sara Mainardi², Hein te Riele³, Roderick L. Beijersbergen², Wenxin Qin^{1*}, Leila Akkari^{3*} & René Bernards^{2*}

Liver cancer remains difficult to treat, owing to a paucity of drugs that target critical dependencies^{1,2}; broad-spectrum kinase inhibitors such as sorafenib provide only a modest benefit to patients with hepatocellular carcinoma³. The induction of senescence may represent a strategy for the treatment of cancer, especially when combined with a second drug that selectively eliminates senescent cancer cells (senolysis)^{4,5}. Here, using a kinome-focused genetic screen, we show that pharmacological inhibition of the DNA-replication kinase CDC7 induces senescence selectively in liver cancer cells with mutations in TP53. A follow-up chemical screen identified the antidepressant sertraline as an agent that kills hepatocellular carcinoma cells that have been rendered senescent by inhibition of CDC7. Sertraline suppressed mTOR signalling, and selective drugs that target this pathway were highly effective in causing the apoptotic cell death of hepatocellular carcinoma cells treated with a CDC7 inhibitor. The feedback reactivation of mTOR signalling after its inhibition⁶ is blocked in cells that have been treated with a CDC7 inhibitor, which leads to the sustained inhibition of mTOR and cell death. Using multiple in vivo mouse models of liver cancer, we show that treatment with combined inhibition of CDC7 and mTOR results in a marked reduction of tumour growth. Our data indicate that exploiting an induced vulnerability could be an effective treatment for liver cancer.

The increase in the incidence of hepatocellular carcinoma (HCC)², the fact that HCC mutations cannot currently be treated with drugs, and unresponsiveness of these tumours to therapy highlight the urgent need to develop new therapeutic approaches for treating this disease⁷. A ‘one–two punch’ approach to cancer therapy has previously been proposed, in which the first drug induces a vulnerability that is exploited by the second drug^{4,5}. Senescent cells have distinct cellular features, which can confer sensitivity to senolytic agents^{8,9}. Here we experimentally validate the one–two punch therapy for treatment of liver cancer with mutations in TP53.

To identify genes that, when inactivated, can induce senescence in liver cancer cells, we used a CRISPR–Cas9 genetic screen with a lentiviral guide RNA (gRNA) library that represents all human kinases in Hep3B and Huh7 liver cancer cells¹⁰ (Fig. 1a). We identified 38 genes that are required for proliferation (Fig. 1b, Extended Data Fig. 1a, Supplementary Table 1), 14 of which could be inhibited by small-molecule compounds (Fig. 1b). We screened compounds that target these 14 kinases for their ability to induce senescence selectively in liver cancer cells (Fig. 1c). XL413—a potent inhibitor of the DNA-replication kinase CDC7¹¹—was the most selective of these compounds in inducing senescence-associated β -galactosidase (SA- β -gal, a marker of senescence) in Hep3B and Huh7 cells, as compared to non-transformed BJ and RPE-1 human cell lines (Fig. 1c). These findings suggest that the

inhibition of CDC7 could represent a senescence-inducing strategy in liver cancer.

As seen in several types of tumour¹², liver cancer cell lines express levels of CDC7 that are higher than those of non-transformed cells (Extended Data Fig. 1b). Expression of CDC7 is upregulated in tumour tissues relative to paired non-tumour tissues in two cohorts of patients with liver cancer ($n = 213$ and $n = 50$) (Fig. 1d), and this was confirmed at the protein level (Extended Data Fig. 1c). Moreover, in a cohort of 365 patients with HCC¹³, patients with the highest levels of CDC7 mRNA in their tumours exhibited the worst survival (Extended Data Fig. 1d).

We treated a panel of non-transformed cells and liver cancer cell lines with increasing concentrations of XL413. Proliferation was impaired in liver cancer cell lines with mutations in TP53, whereas liver cancer cell lines with wild-type TP53 (SK-Hep1 and Huh6 cells)—as well as all four non-transformed cell lines—displayed no sensitivity to XL413 (Fig. 2a). The XL413-sensitive cell line HepG2 is an outlier in this respect but carries a mutation in ATM, which acts upstream of p53 in the DNA-damage response. Importantly, knockdown of TP53 mediated by short hairpin RNA (shRNA) in wild-type cells sensitized these cells to CDC7 inhibition (Extended Data Fig. 1e–g), which indicates a causal relationship between TP53 mutation status and sensitivity to inhibition of CDC7.

The anti-proliferative effect of XL413 was associated with the induction of senescence markers in liver cancer cells with TP53 mutations, but not in liver cancer cells with wild-type TP53 or in non-transformed cells (Fig. 2b, Extended Data Fig. 2a), and a senescence signature¹⁴ was enriched in HCC cells with mutations in TP53 treated with XL413 (Fig. 2c). The notion that CDC7 inhibition induces a senescence-like state in liver cancer cells with mutations in TP53 is further supported by the findings that (i) withdrawal of XL413 does not lead to re-entry into the cell cycle in the majority of HCC cells, (ii) treatment with XL413 induced senescence-associated heterochromatin foci and (iii) treatment with XL413 induced expression of a number of cytokines, as part of the senescence-associated secretory phenotype¹⁵ (Extended Data Fig. 2b–d). There was no evidence for substantial induction of apoptosis in HCC cells with TP53 mutations treated with XL413 (Extended data Fig. 2e). Comparable results were obtained with two CDC7 inhibitors that are unrelated to XL413—LY3177833 and TAK-931 (Extended Data Fig. 3a–f). Consistent with this, knockdown of CDC7 impaired proliferation and induced senescence in liver cancer cells with TP53 mutations, but had no effect on cells with wild-type TP53 (Extended Data Fig. 3g–i).

The phosphorylation of MCM2 (a target of CDC7¹²) was suppressed equally by each of the three CDC7 inhibitors in both wild-type cells and cells with TP53 mutations (Fig. 2d, Extended Data Fig. 4a, b),

¹State Key Laboratory of Oncogenes and Related Genes, Shanghai Cancer Institute, Renji Hospital, Shanghai Jiao Tong University School of Medicine, Shanghai, China. ²Onco Institute, Division of Molecular Carcinogenesis, The Netherlands Cancer Institute, Amsterdam, The Netherlands. ³Onco Institute, Division of Tumour Biology and Immunology, The Netherlands Cancer Institute, Amsterdam, The Netherlands. ⁴Division of Cell Biology, The Netherlands Cancer Institute, Amsterdam, The Netherlands. ⁵Liver Cancer Institute, Zhongshan Hospital, Fudan University, Key Laboratory of Carcinogenesis and Cancer Invasion, Ministry of Education, Shanghai, China. ⁶Department of Pathology, Eastern Hepatobiliary Surgery Hospital, Second Military Medical University, Shanghai, China. ⁷These authors contributed equally: Cun Wang, Serena Vegna, Haojie Jin, Bente Benedict. *e-mail: wxqin@sjtu.edu.cn; lakkari@nki.nl; rbernards@nki.nl

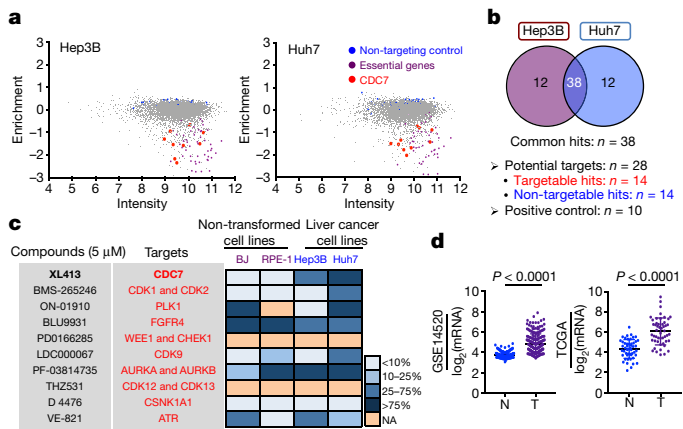


Fig. 1 | A two-step screen identifies CDC7 as a target for the senescence-inducing strategy in liver cancer. **a**, Hep3B and Huh7 cells were transduced with a lentiviral kinome gRNA library and 3 independent replicates were cultured for 14 days. gRNA barcodes from samples at day 0 and day 14 were recovered by PCR, and analysed by next-generation sequencing. The y axis shows \log_2 scale in abundance (ratio of gRNA frequency in the day-14 sample to that in the day-0 sample). The x axis shows \log_2 scale of the average read-count in the samples of day 0. **b**, Thirty-eight common hits (among the top 50 most-strongly depleted hits in each cell line) were identified by CRISPR screen in Hep3B and Huh7 cells. **c**, Heat map indicates the effects of compounds (10 compounds targeting 14 hits identified by CRISPR screen, 5 μM for 4-day treatments) on inducing SA- β -gal activity in non-transformed cell lines (BJ and RPE-1) and liver cancer cell lines (Hep3B and Huh7). NA, not applicable. **d**, CDC7 mRNA expression in paired tumour (T) and non-tumour (N) tissues from GSE14520 cohort ($n = 213$ patients) and The Cancer Genome Atlas (TCGA) database ($n = 50$ patients). Paired two-sided t -test. Data in graphs are mean \pm s.d. Data in a–c are representative of three independent biological experiments.

which indicates that there is no correlation between the cell fate that is induced by CDC7 inhibitors and the degree of inhibition of the downstream targets of CDC7. To further address why it is that inhibition of CDC7 selectively induces senescence in the context of TP53 mutation, we assessed protein expression associated with DNA damage following treatment with XL413. The induction of γ H2AX and DNA double-strand breaks was notable after CDC7 inhibition in liver cancer cells with TP53 mutations as compared to cells with wild-type TP53; these latter instead displayed a clear upregulation of p21 (CIP1) (Fig. 2d, e, Extended Data Fig. 4a–c). This differential effect is most readily explained by the finding that multiple gene signatures associated with DNA repair are upregulated in cells with wild-type TP53 (SK-Hep1 and BJ) treated with XL413, but are suppressed in cells with TP53 mutations upon inhibition of CDC7 (Fig. 2f, Extended Data Fig. 4d, e). Consistently, the inhibition of DNA repair with the ATR inhibitor AZD6738, or with the CHK1 inhibitor MK-8776, in liver cancer cells with wild-type TP53 resulted in increased double-strand breaks when combined with treatment with XL413 (Extended Data Fig. 4f). Inhibition of CDC7 also resulted in a significant increase in the duration of mitosis (Extended Data Fig. 4g, h). We further confirmed the specificity of the effects of CDC7 inhibition in *Trp53*^{-/-} mouse cell models of liver cancer¹⁶ (Extended Data Fig. 4i, j). Moreover, XL413 induced senescence in non-small-cell lung-cancer cells with TP53 mutations, but not in cells with wild-type TP53 (Extended Data Fig. 5a, b). Similarly, in isogenic TP53^{-/-} and TP53^{+/+} HCT116 colon-cancer cells, the inhibition of CDC7 induced senescence only in TP53^{-/-} cells (Extended Data Fig. 5c–e).

The induction of senescence represents a double-edged sword for tumour control^{15,17}, and the potentially harmful properties of senescent tumour cells make their elimination therapeutically relevant. The high concentration of ABT263⁸, a senolytic BH3 mimetic drug, that is required to promote apoptosis of XL413-induced senescent cells—and the lack of sensitivity of these cells to dasatinib⁹—prevent their

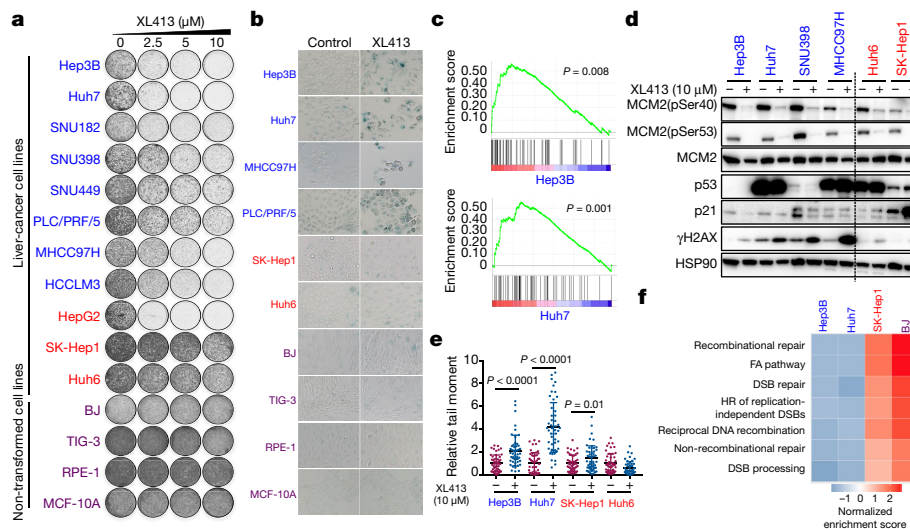


Fig. 2 | Inhibition of CDC7 selectively induces senescence in liver cancer cells with TP53 mutations. **a**, Long-term colony formation assay was performed over 10–14 days on liver cancer cell lines with TP53 mutations (blue), liver cancer cell lines with wild-type TP53 (red) and non-transformed cell lines (purple), cultured with the indicated concentrations of XL413. **b**, Liver cancer cells and non-transformed cell lines were cultured in the presence of 10 μM XL413 for 4 days and the induction of senescence was assessed by staining for SA- β -gal activity. **c**, GSEA of a previously published¹⁴ signature of genes that are upregulated in senescence, in sequencing data from Hep3B and Huh7 cells treated with 10 μM XL413 for 4 days (Methods). **d**, Proteins were extracted from liver cancer cell lines with TP53 mutations or wild-type TP53, treated with 10 μM XL413 for 7 days and then analysed by western blotting.

MCM2(pSer40), MCM2 phosphorylated at Ser40; MCM2(pSer53), MCM2 phosphorylated at Ser53. **e**, Neutral comet assays were performed on Hep3B, Huh7, SK-Hep1 and Huh6 cells cultured with 10 μM XL413 for 7 days. The value of tail moments in each treatment group were normalized on the basis of the mean value of the control cells. $n = 50$ cells per cell line and condition. Data in graphs are mean \pm s.d., analysed by unpaired two-sided t -test. **f**, GSEA in cells with TP53 mutations (Hep3B and Huh7 cells) or wild-type TP53 (SK-Hep1 and BJ cells), treated with 10 μM XL413 for 4 days. DSB, double-strand break; FA, Fanconi anaemia; HR, homologous recombination. For gel source images, see Supplementary Fig. 1. Data in a, b are representative of three independent biological experiments. Data in d, e are representative of two independent biological experiments.

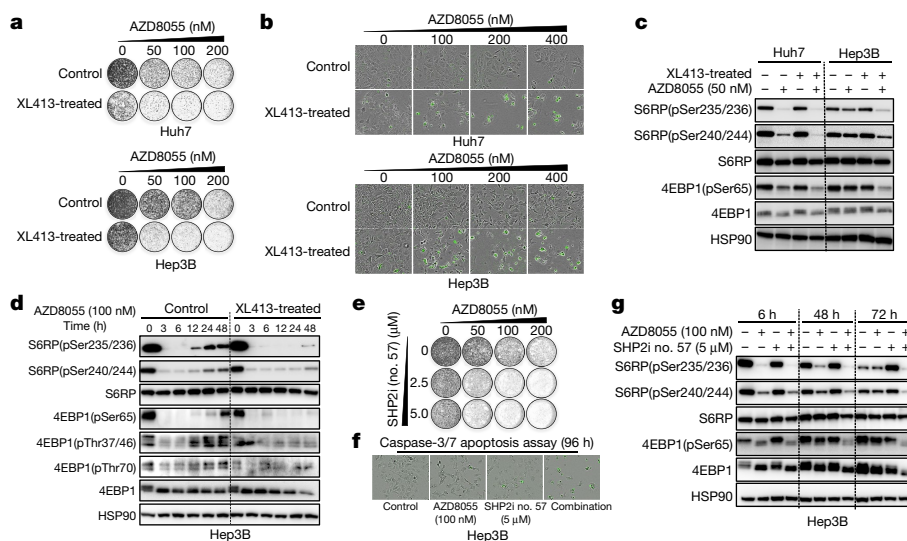


Fig. 3 | AZD8055 selectively triggers apoptosis in XL1413-induced senescent cells. **a**, Hep3B and Huh7 cells were treated with 10 μ M XL1413 or vehicle for 10 days, before sequential exposure to increasing concentrations of AZD8055 for 5–7 days in colony-formation assays. **b**, Apoptotic cells were determined by caspase-3 and caspase-7 (caspase-3/7) apoptosis assay, 96 h after treatment with AZD8055. **c**, Control cells and XL1413-induced senescent cells were treated with AZD8055 for 48 h before western blot analyses with the indicated antibodies. S6RP(pSer235/236), S6RP phosphorylated at Ser235 and Ser236; S6RP(pSer240/244), S6RP phosphorylated at Ser240 and Ser244; 4EBP1(pSer65), 4EBP1 phosphorylated at Ser65. **d**, Control cells and XL1413-induced senescent cells were treated with AZD8055, and cell lysates

were collected at the indicated time points before western blot analyses with the indicated antibodies. 4EBP1(pThr37/46), 4EBP1 phosphorylated at Thr37 and Thr46; 4EBP1(pThr70), 4EBP1 phosphorylated at Thr70. **e**, **f**, Long-term colony formation assays, and caspase-3 and caspase-7 apoptosis assays, showing the synergistic effect of mTOR and SHP2 inhibitors on the proliferation of Hep3B cells. SHP2i no. 57, SHP2 inhibitor (compound no. 57; Methods). **g**, Hep3B cells were treated with AZD8055, SHP2 inhibitor or a combination of both drugs at the indicated time points, before western blot analysis with the indicated antibodies. For gel source images, see Supplementary Fig. 1. Data in **a–f** are representative of three independent biological experiments. Data in **g** are representative of two independent biological experiments.

translational use in the clinic (data not shown). We therefore sought to identify less-toxic compounds to selectively kill senescent liver cancer cells using a library screen of G-protein-coupled receptor (GPCR) compounds in proliferating and in XL1413-treated senescent Huh7 cells (Extended Data Fig. 6a). Of these compounds, only the anti-depressant sertraline exhibited differential effects on proliferating versus XL1413-induced senescent cells (Extended Data Fig. 6b, c); sertraline had modest effects on proliferating cells, but induced substantial apoptosis after treatment with XL1413 (Extended Data Fig. 6d–f).

The concentration of sertraline needed to induce apoptosis of senescent cells precludes its clinical use. We therefore explored the mechanism through which sertraline selectively induces apoptosis in XL1413-treated senescent cells. We analysed signalling pathways in cells treated with sertraline, and found that this treatment leads to inhibition of S6RP and 4EBP1 phosphorylation in XL1413-induced senescent cells (Extended Data Fig. 6g). This suggests that the apoptotic effects of sertraline may involve regulation of mTOR signalling, as has previously been reported¹⁸. Consistently, gene-set enrichment analyses (GSEA) on RNA-sequencing data from cells treated sequentially with XL1413 and sertraline indicated the enrichment of a gene set related to the downregulation of mTOR signalling (Extended Data Fig. 6h).

To explore whether mTOR inhibitors may be used as effective drugs in our XL1413-induced senescence models, we analysed the activity of two mTOR inhibitors (AZD8055 and AZD2014). Both of these inhibitors induced apoptosis in XL1413-treated liver- and lung cancer cells with *TP53* mutations, but only limiting the proliferation of untreated cells (Fig. 3a, b, Extended Data Fig. 6i–k). As expected, sequential treatment with AZD8055 did not lead to apoptosis in non-senescent liver cancer cells with wild-type *TP53* that were pre-treated with XL1413 (Extended Data Fig. 6l). Importantly, mTOR signalling was further inhibited in XL1413-induced senescent cells exposed to AZD8055 or AZD2014, as compared to proliferating cells (Fig. 3c, Extended Data Fig. 6m).

mTOR blockade results in a feedback-loop reactivation of mTOR signalling through the engagement of receptor tyrosine kinases, which

thus limits the efficacy of mTOR inhibitors⁶. We explored the feedback activation of mTOR signalling in time-course experiments, and found that the rapid reactivation of mTOR—as judged by the phosphorylation of S6RP and 4EBP1 at multiple sites—was observed in proliferating, but not in senescent, Hep3B cells (Fig. 3d). This feedback reactivation loop may stem from both transcriptional and biochemical activation of EGFR, PDGFR β and IGF-1R, which leads to an increase in the phosphorylation of SHP2—this latter process is disrupted in Hep3B cells treated with XL1413 (Extended Data Fig. 7a–c). Combining mTOR and SHP2 inhibitors resulted in an inhibition of the feedback reactivation of mTOR signalling and caused cell death in proliferating Hep3B cells (Fig. 3e–g), which indicates that suppression of mTOR reactivation is critical for the induction of apoptosis in senescent cells. In support of these findings, inhibition of mTOR also induced the activation of AKT in proliferating cells, and inhibition of AKT synergized with mTOR blockade to induce cell death (Extended Data Fig. 7d–f). Oncogene-induced senescent primary fibroblasts were insensitive to treatment with AZD8055 (Extended Data Fig. 8a, b), which indicates that not all senescent cells are killed by inhibition of mTOR. Importantly, feedback reactivation of mTOR was not impaired in cisplatin- or alisertib-induced senescent Hep3B cells and, consequently, no cell death was observed following the inhibition of mTOR in these cells (Extended Data Fig. 8c–e). These data indicate that the efficacy of mTOR inhibitors is dependent on context, and relies on CDC7 inhibition.

To assess whether our *in vitro* findings could be recapitulated *in vivo*, we generated Huh7 and MHCC97H xenografts. XL1413-treated tumours showed increased DNA damage and SA- β -gal⁺ senescent cells as compared to tumours treated with vehicle, AZD8055 or a combination of XL1413 and AZD8005, which indicates that the inhibition of CDC7 induces senescence *in vivo* (Extended Data Fig. 9a). No SA- β -gal staining was observed in SK-Hep1 tumours with wild-type *TP53* that were treated with XL1413, which is consistent with the notion that the inhibition of CDC7 induces senescence only in a background of *TP53* mutation (Extended Data Fig. 9b). Compared to treatment with sorafenib, treatment with a combination of XL1413 and AZD8055

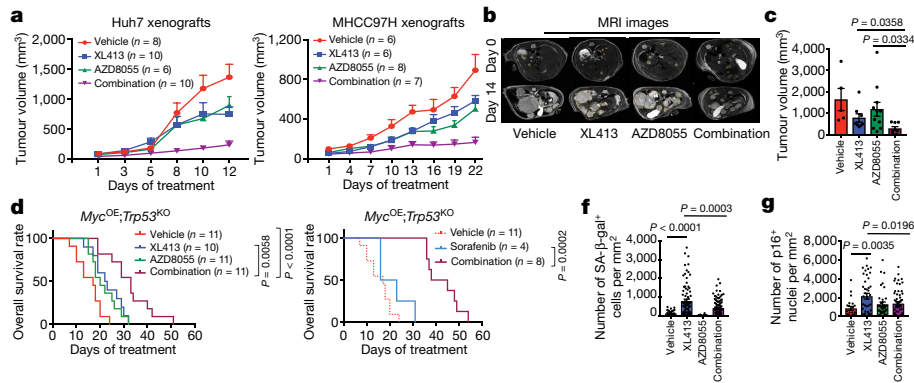


Fig. 4 | Inhibition of CDC7 induces senescence in vivo, and suppresses tumour growth when combined with mTOR inhibition in multiple models of liver cancer. **a**, Huh7 and MHCC97H cells were grown as tumour xenografts in BALB/c nude mice. Longitudinal progression of tumour volume in mice bearing Huh7 and MHCC97H tumours that were treated for 12 or 22 days, respectively, with vehicle, XL413, AZD8055 or both drugs combined. Graph shows mean \pm s.e.m. **b–g**, Analyses of response to treatment with both drugs in the *Myc*^{OE};*Trp53*^{KO} somatic mouse model of HCC. **b**, Representative magnetic resonance imaging (MRI) images out of nine independent experimental cohorts, of day 0 and day 14 of mice enrolled in treatment with vehicle, XL413, AZD8055 or a combination of both drugs. The yellow line indicates the visible tumour area that was used to calculate the tumour volume. **c**, Tumour volumes were calculated on the basis of MRI images from mice bearing HCC with a matched initial tumour volume. Graph shows mean \pm s.e.m. from

mice treated with vehicle ($n = 5$), XL413 ($n = 8$), AZD8055 ($n = 11$) or a combination of the two drugs ($n = 8$) at the intermediate time point after the initiation of treatment (days 14–16 in matched treatment groups). Unpaired two-sided *t*-test. **d**, Survival curve generated from mice bearing *Myc*^{OE};*Trp53*^{KO} tumours, treated with vehicle ($n = 11$; median survival 17 days), XL413 ($n = 10$; median survival of 22.5 days), AZD8055 ($n = 11$; median survival of 20 days) or a combination of the two drugs ($n = 11$; median survival of 33 days). **e**, Survival curve generated from independent cohorts of mice bearing *Myc*^{OE};*Trp53*^{KO} HCC, treated with sorafenib ($n = 4$; median survival of 19.5 days) or a combination of XL413 and AZD8055 ($n = 8$; median survival of 41.5 days). The vehicle group from **d** is used as a reference. **d**, **e**, Statistical significance was calculated using a two-sided log-rank test. **f**, **g**, Graphs show mean \pm s.e.m. of the number of SA- β -gal⁺ (**f**) or p16⁺ (**g**) cells per tumour nodule per mm². Unpaired two-sided *t*-test. For sample sizes, see Methods.

elicited a more-effective inhibition of growth, and combination-treated xenografts with *TP53* mutations displayed diminished proliferation and phosphorylation of 4EBP1 that was associated with increased apoptosis (Fig. 4a, Extended Data Fig. 9c–g).

In immune-competent, somatic mouse models of HCC¹⁹ (Extended Data Fig. 10a), treatment with XL413 induced senescence specifically in *Trp53*-deficient tumours (overexpression of *Myc* and knockout of *Trp53*; *Myc*^{OE};*Trp53*^{KO}) but not in *Myc*^{OE};*Pten*^{KO} tumours (Extended Data Fig. 10b). Mice bearing *Myc*^{OE};*Trp53*^{KO} tumours that received XL413 or AZD8055 monotherapy showed a modest reduction in tumour volume and increased mouse lifespan, whereas treatment with XL413 combined with AZD8055 was well-tolerated, significantly reduced tumour burden and increased survival compared to either monotherapy or to treatment with sorafenib in this model of aggressive HCC (Fig. 4b–e, Extended Data Fig. 10c–f). Importantly, the number of SA- β -gal⁺ and p16 (INK4A)⁺ cells was decreased in the combination-treated group, which suggests that senescent cells were efficiently eliminated by treatment with AZD8055 (Fig. 4f, g, Extended Data Fig. 10g, h). An influx of macrophages (CD11b⁺Ly6C⁺Ly6G⁻), CD4⁺ T cells and increased proliferation of CD4⁺ and CD8⁺ T cells were observed after treatment with XL413 at the intermediate time-point of treatment. These changes were largely lost in the combination-treated groups, and in XL413-treated endpoint tumours (Extended Data Fig. 10i). Withdrawal of XL413 after the induction of senescence in vivo did not alter the absolute number of senescent cells, which suggests that infiltrating immune cells were unable to efficiently clear senescent cells (Extended Data Fig. 10j).

Our data indicate that pro-senescence therapy with a CDC7 inhibitor, combined with mTOR inhibitor, may deliver clinical benefit in liver cancer by alleviating both the cell-autonomous²⁰ and non-cell-autonomous²¹ attributes of senescent cells—thus reducing the risk of tumour relapse. Although immune surveillance was mobilized, it had limited effect after inhibition of CDC7. It will be worthwhile to investigate whether combining immunotherapy (which has demonstrated activity in HCC²²) with pro-senescence therapy can activate the cytotoxic potential of recruited immune cells in tumours that have been treated with pro-senescence therapy.

Online content

Any methods, additional references, Nature Research reporting summaries, source data, extended data, supplementary information, acknowledgements, peer review information; details of author contributions and competing interests; and statements of data and code availability are available at <https://doi.org/10.1038/s41586-019-1607-3>.

Received: 18 October 2018; Accepted: 21 August 2019;
Published online 2 October 2019.

- Bray, F. et al. Global cancer statistics 2018: GLOBOCAN estimates of incidence and mortality worldwide for 36 cancers in 185 countries. *CA Cancer J. Clin.* **68**, 394–424 (2018).
- Llovet, J. M. et al. Hepatocellular carcinoma. *Nat. Rev. Dis. Primers* **2**, 16018 (2016).
- Llovet, J. M. et al. Sorafenib in advanced hepatocellular carcinoma. *N. Engl. J. Med.* **359**, 378–390 (2008).
- Wang, L. et al. High-throughput functional genetic and compound screens identify targets for senescence induction in cancer. *Cell Reports* **21**, 773–783 (2017).
- Sieben, C. J., Sturmlechner, I., van de Sluis, B. & van Deursen, J. M. Two-step senescence-focused cancer therapies. *Trends Cell Biol.* **28**, 723–737 (2018).
- Rodrik-Outmezguine, V. S. et al. mTOR kinase inhibition causes feedback-dependent biphasic regulation of AKT signaling. *Cancer Discov.* **1**, 248–259 (2011).
- Zucman-Rossi, J., Villanueva, A., Nault, J. C. & Llovet, J. M. Genetic landscape and biomarkers of hepatocellular carcinoma. *Gastroenterology* **149**, 1226–1239 (2015).
- Chang, J. et al. Clearance of senescent cells by ABT263 rejuvenates aged hematopoietic stem cells in mice. *Nat. Med.* **22**, 78–83 (2016).
- Ogrodnik, M. et al. Cellular senescence drives age-dependent hepatic steatosis. *Nat. Commun.* **8**, 15691 (2017).
- Wang, C. et al. A CRISPR screen identifies CDK7 as a therapeutic target in hepatocellular carcinoma. *Cell Res.* **28**, 690–692 (2018).
- Koltun, E. S. et al. Discovery of XL413, a potent and selective CDC7 inhibitor. *Bioorg. Med. Chem. Lett.* **22**, 3727–3731 (2012).
- Montagnoli, A., Moll, J. & Colotta, F. Targeting cell division cycle 7 kinase: a new approach for cancer therapy. *Clin. Cancer Res.* **16**, 4503–4508 (2010).
- Cancer Genome Atlas Research Network. Comprehensive and integrative genomic characterization of hepatocellular carcinoma. *Cell* **169**, 1327–1341 (2017).
- Fridman, A. L. & Tainsky, M. A. Critical pathways in cellular senescence and immortalization revealed by gene expression profiling. *Oncogene* **27**, 5975–5987 (2008).
- Faget, D. V., Ren, Q. & Stewart, S. A. Unmasking senescence: context-dependent effects of SASP in cancer. *Nat. Rev. Cancer* **19**, 439–453 (2019).

16. Dauch, D. et al. A MYC-aurora kinase A protein complex represents an actionable drug target in p53-altered liver cancer. *Nat. Med.* **22**, 744–753 (2016).
17. Eggert, T. et al. Distinct functions of senescence-associated immune responses in liver tumor surveillance and tumor progression. *Cancer Cell* **30**, 533–547 (2016).
18. Lin, C. J., Robert, F., Sukarieh, R., Michnick, S. & Pelletier, J. The antidepressant sertraline inhibits translation initiation by curtailing mammalian target of rapamycin signaling. *Cancer Res.* **70**, 3199–3208 (2010).
19. Keng, V. W. et al. A conditional transposon-based insertional mutagenesis screen for genes associated with mouse hepatocellular carcinoma. *Nat. Biotechnol.* **27**, 264–274 (2009).
20. Milanovic, M. et al. Senescence-associated reprogramming promotes cancer stemness. *Nature* **553**, 96–100 (2018).
21. Georgilis, A. et al. PTBP1-mediated alternative splicing regulates the inflammatory secretome and the pro-tumorigenic effects of senescent cells. *Cancer Cell* **34**, 85–102 (2018).
22. Flynn, M. J., Sayed, A. A., Sharma, R., Siddique, A. & Pinato, D. J. Challenges and opportunities in the clinical development of immune checkpoint inhibitors for hepatocellular carcinoma. *Hepatology* **69**, 2258–2270 (2019).

Publisher's note Springer Nature remains neutral with regard to jurisdictional claims in published maps and institutional affiliations.

© The Author(s), under exclusive licence to Springer Nature Limited 2019

METHODS

No statistical methods were used to predetermine sample size. The experiments were not randomized and investigators were not blinded to allocation during experiments and outcome assessment.

Cell lines. The human liver cancer cell lines, Hep3B, Huh7, HepG2, SNU182, SNU398, SNU449, Huh6, SK-Hep1 and PLC/PRF/5 were provided by Erasmus University. MHCC97H and HCCLM3 were provided by the Liver Cancer Institute of Zhongshan Hospital. The majority of liver cancer cell lines were established from HCC. Among these cell lines, SK-Hep1 was established from an endothelial tumour in the liver and Huh6 is a hepatoblastoma cell line. Liver cancer cells were cultured in DMEM with 10% FBS, glutamine and penicillin–streptomycin (Gibco) at 37 °C and 5% CO₂. The liver cancer cell lines were authenticated by applying short-tandem-repeat DNA profiling. HCT116 (*TP53*^{+/+} and *TP53*^{-/-}) cells were provided by B. Vogelstein. hTERT immortalized BJ fibroblasts and retinal pigment epithelial cells (RPE-1) were provided by X. Qiao (Netherlands Cancer Institute). TIG-3 immortalized with hTERT and MCF-10A cells were provided by L. Li (Netherlands Cancer Institute). Two mouse cell models of liver cancer with different genetic backgrounds (*Nras*^{G12V}; *Myc*^{OE}; *Trp53*^{-/-} and *Nras*^{G12V}; *Myc*^{OE}; *Cdkn2a*^{ARF-/-}) were provided by L. Zender (University Hospital Tubingen). Mycoplasma contamination was excluded using a PCR-based method.

Compounds and antibodies. XL413 (S7547), BMS265246 (S2014), ON-01910 (S1362), PD0166285 (S8148), LDC000067 (S7461), PF-03814735 (S2725), D 4476 (S7642), VE-821 (S8007), AZD8055 (S1555), AZD2014 (S2783), AZD6738 (S7693) and MK-8776 (2735) were purchased from Selleck Chemicals. THZ531 (A8736) was purchased from ApexBio. XL413 (205768), BLU9931 (206192) and LY3177833 (206762) were purchased from MedKoo. TAK-931 (CT-TAK931) was purchased from Chemietek. XL413 (A13677) was also purchased from AduoQ BIOSCIENCE. The SHP2 inhibitor used in this study is covered by a patent application (WO 2015/107495A1; compound no. 57) and was synthesized as previously described²³.

Antibodies against HSP90 (sc-7947, sc-13119), p53 (sc-126), p21 (sc-6246), and SHP2 (sc-280) were purchased from Santa Cruz Biotechnology. Antibodies against CDC7 (ab77668), p-MCM2 (ab109133, ab133243), MCM2 (ab4461), p-SHP2 (ab62322), PCNA (ab2426), and cleaved caspase-3 (ab2303) were purchased from Abcam. Antibodies against γ H2AX (no. 9718), p-S6RP (no. 4856, no. 5364), S6RP (no. 2317), p-4EBP1 (no. 9456, no. 2855, no. 9455), 4EBP1 (no. 9644), p-IGF-1R/INSR (no. 3024), IGF-1R (no. 9750), p-PDGFR β (no. 3161), PDGFR β (no. 4564), p-AKT (no. 4060) and AKT (no. 2920) were purchased from Cell Signalling. EGFR antibody (610017) was purchased from BD Biosciences. H3K9me3 antibody (49-1008) and p-EGFR (44-788) were from Thermo Fisher Scientific.

Pooled 'stress lethal' CRISPR screen. For the design of the kinome CRISPR library, 5,971 gRNAs targeting 504 human kinases, 10 essential genes and 50 non-targeting gRNAs were selected. Oligonucleotides with gRNA sequences flanked by adaptors were ordered from CustomArray, and cloned as a pool by GIBSON assembly in LentiCRISPRv2.1. The kinome CRISPR library was introduced to Hep3B and Huh7 cells by lentiviral transduction. Cells stably expressing gRNA were cultured for 14 days. The abundance of each gRNA in the pooled samples was determined by Illumina deep-sequencing. gRNAs prioritized for further analysis were selected by the fold depletion of abundance in the day-14 sample compared with that in the day-0 sample, using previously described methods²⁴.

Compound screens. Induction of senescence screen. We performed a compound screen including 10 small-molecule inhibitors that targeting the 14 hits identified in the CRISPR screen. The compounds used for this screen are described in Fig. 1c. Each compound was evaluated in two liver cancer cell lines (Hep3B and Huh7) and two non-transformed cell lines (BJ and RPE-1) using five different concentrations. The screens were performed in three replicates of each cell line. SA- β -gal staining was performed after 4 days of treatment.

Killing senescent-cell screen. Cells were screened for sensitivity against a panel of 260 small-molecule inhibitors from a GPCR compound library (L2200, Selleck Chemicals). In brief, Huh7 cells were treated with 10 μ M XL413 for 5 days, and then control cells and XL413-treated cells were plated in 96-well plates. All compounds from GPCR library were tested at four concentrations. Each plate included 8 wells containing DMSO (as a negative control) and 8 wells containing 10 μ M PAO (as a positive control). The cell viability in each well was determined using CellTiter-Blue reagent (Promega). The relative survival of control cells and XL413-treated senescent cells in the presence of drug was normalized against control conditions (untreated cells) after subtraction of background signal.

SA- β -gal staining. SA- β -gal staining was performed either in 6-well or 96-well plates (for in vitro studies), on 10- μ m-thick cryosections from xenografted tumours or on 8- μ m-thick cryosections from hydrodynamic-tail-vein-injection (HDTVi)-generated *Myc*^{OE}; *Trp53*^{KO} tumours, using a commercial kit (Sigma) following the manufacturer's instructions.

Protein lysate preparation and western blots. Cells were washed with PBS and lysed with RIPA buffer supplemented with complete protease inhibitor (Roche) and phosphatase inhibitor cocktails II and III (Sigma). Protein quantification was

performed with the BCA protein assay kit (Pierce). All lysates were freshly prepared and processed with Novex NuPAGE gel electrophoresis systems (Thermo Fisher Scientific), followed by western blotting.

Immunohistochemical staining. Specimens of HCC were obtained from 80 patients (from 26 to 76 years old) who underwent curative surgery in Eastern Hepatobiliary Hospital of the Second Military Medical University. Patients were not subject to any preoperative anti-cancer treatment. Ethical approval was obtained from the Eastern Hepatobiliary Hospital Research Ethics Committee, and written informed consent was obtained from each patient. Of these cases, 12 patients are female and 68 patients are male. Fifty-nine patients had a background of HBV infection. Clinical information—including tumour number, diameter of tumour, tumour differentiation, serum AFP, status of cancer recurrence, disease-free survival and death from recurrence—was collected. For immunohistochemical analysis, formalin-fixed paraffin-embedded samples from patients with HCC were probed with CDC7 antibody (ab77668, Abcam). Formalin-fixed paraffin-embedded samples were also obtained from xenograft tumours or tumours from immunocompetent somatic mouse models, and then probed with antibodies against PCNA (ab2426, Abcam), cleaved caspase-3 (ab2303, Abcam), p-4EBP1 (no. 2855, Cell Signaling) or p16 (ab54210, Abcam). Following incubation with the primary antibodies, positive cells were visualized using DAB+ as a chromogen. For the analysis of p16 and SA- β -gal staining, slides were digitally processed using the Aperio ScanScope (Aperio) at a magnification of 20 \times . Nodule size was drawn by hand in HALO image-analysis software (Indica Labs) and an algorithm was designed with the Multiplex IHC v.1.2 module to quantify the number of positive cells²⁵ either as absolute or per mm² (as indicated in figure legends).

Long-term cell-proliferation assays (colony formation). Cells were cultured and seeded into 6-well plates at a density of 5×10^3 to 4×10^4 cells per well, depending on growth rate, and were cultured in medium containing the indicated drugs for 10–14 days. The medium was changed twice a week. Cells were fixed with 4% formaldehyde in PBS and stained with 0.1% crystal violet diluted in water.

Plasmids. All lentiviral shRNA vectors were retrieved from the arrayed The RNAi Consortium human genome-wide shRNA collection. These shRNAs were as follows: *CDC7* shRNA no. 1: TRCN000003168_CCGGGCCA CAGCACAGTTACAAGTACTCGAGTACTGTAACTGTGCTG TGGCTTTT; *CDC7* shRNA no. 2: TRCN000196542_CCGGGAAGCTTTGTTGCAT CCATTTCT CGAGAAATGGATGCAACAAAGCTTCTTTTGTG; *TP53* shRNA no. 1: TRCN000010814_CCGGGAGGGATGTTTGGGA GATGTACTCGAGTACA TCTCCCAAACATCCCTCTTTT; *TP53* shRNA no. 2: TRCN000003754_CCGGTCAGACCTATGGAAACTACTTCTCGAGAAGT AGTTTCCATAGGTCTGATTTT; and *TP53* shRNA no. 3: TRCN000003755_CCGGTCAGATGAAGCTCCAGAATC GAGTCTGGAGCTCATCT GGACTTTTT

Incucyte cell-proliferation assay and apoptosis assay. Indicated cell lines were seeded into 96-well plates at a density of 1,000–8,000 cells per well, depending on growth rate and the design of the experiment. About 24 h later, drugs were added at the indicated concentrations using the HP D300 Digital Dispenser (HP). Cells were imaged every 4 h using the Incucyte ZOOM (Essen Bioscience). Phase-contrast images were analysed to detect cell proliferation on the basis of cell confluence. For cell apoptosis, caspase-3 and caspase-7 green apoptosis-assay reagent was added to the culture medium, and cell apoptosis was analysed on the basis of green fluorescent staining of apoptotic cells.

RNA sequencing. RNA (one sample per cell line per condition) was isolated using Trizol, and cDNA libraries were sequenced on an Illumina HiSeq2500 to obtain 65-bp single-end sequence reads. Reads were aligned to the GRCh38 human reference genome. GSEA was performed using GSEA software as previously described²⁶. The 'FRIDMAN_SENESCENCE_UP'¹⁴ gene set was used to assess the enrichment of senescence-associated genes in XL413-treated versus control cells. Gene sets related to DNA-damage repair were used to assess the enrichment of genes associated with DNA-damage repair in the XL413-treated versus control cells. Enrichment scores were corrected for gene-set size (normalized enrichment score). The 'PENG_RAPAMYCIN_RESPONSE_DN'²⁷ gene set was used to assess the enrichment of downregulation of mTOR signalling in liver cancer cells that had been sequentially treated with XL413 and sertraline, versus control cells. The *P* value estimates the statistical significance of the enrichment score for a single gene set, as previously described²⁶. Exact *P* values are shown in the figures, unless the *P* value < 0.001.

Immunofluorescence and image analysis. For immunofluorescence microscopy, cells were seeded on glass coverslips and cultured in the presence of 10 μ M XL413 for 7 days. Cells were fixed in 2% paraformaldehyde and permeabilized with 0.2% Triton X-100 for 5 min, blocked with PBS containing 2% bovine serum albumin (Sigma-Aldrich) for 45 min and subsequently incubated with H3K9me3 antibody (Thermo Fisher Scientific, 49-1008) and goat anti-rabbit Alexa Fluor 488 (Invitrogen; 1:200) for 1 h, respectively. Nuclei were stained with 4,6-diamidino-2-phenylindole. Samples were mounted on glass slides in Mowiol after three

washing steps with PBS. Images were acquired with a Leica TCS SP5 confocal microscope with a 63× (NA 1.4) oil objective. Image processing was performed using ImageJ software.

Neutral comet assay. To detect DNA double-strand breaks, neutral comet assays were performed as previously described²⁸. In brief, cells were collected and embedded in 1% low-gelling-temperature agarose (Sigma-Aldrich). A cell suspension was used to make gels onto comet assay slides (Trevigen). Cells in the agarose gels were lysed at 37°C in lysis buffer (2% sarkosyl, 0.5M Na₂EDTA and 0.5 mg/ml proteinase K) overnight. Subsequently, slides were washed 3 times for 30 min at room temperature in electrophoresis buffer (90 mM Tris-HCl pH 8.5, 90 mM boric acid and 2 mM Na₂EDTA). Electrophoresis was performed for 25 min at 20 V in electrophoresis buffer. Afterwards, slides were washed once with MQ, and DNA was stained using 2.5 µg/ml propidium iodide in MQ. Individual comets were imaged with a Zeiss AxioObserver Z1 inverted microscope. Tail moments of individual comets were assessed using the CASP software. For each condition, at least 50 cells were analysed.

Time-lapse live imaging. To allow visualization of chromosomes, cells were transfected with a histone H2B-GFP (LV-GFP, Addgene plasmid no. 25999). Cells were then plated 24 h before starting the microscope acquisition. XL413 (10 µM) was added in the medium 1 h before starting the movie. Cells were filmed over 96 h and images were taken every 10 min. For each condition filmed, five different fields were selected. In each field, we randomly choose and followed cells entering in mitosis. Nuclear envelope breakdown was used as an indicator of the onset of mitotic division.

Quantitative reverse-transcription PCR. Total RNA was extracted from cells using Trizol reagent from Invitrogen or Quick-RNA MiniPrep from Zymo Research. cDNA synthesis was performed using Maxima Universal First Strand cDNA Synthesis Kit from Thermo Scientific. Quantitative PCR reactions were performed with FastStart Universal SYBR Green Master (Rox) from Roche. The experiments were performed according to the manufacturer's instructions. The sequences of the primers used for quantitative reverse-transcription PCR (RT-qPCR) analyses were as follows: *IL6* forward, ACTCACCTCTTCAGAACGAATTG; *IL6* reverse, CCATCTTTGGAAGGTTTCAGGTTG; *IL8* forward, TTTTGC CAAGGAGTGCTAAAGA; *IL8* reverse, AACCTCTGCACCCAGTTTTC; *MMP1* forward, TTGTGGCCAGAAAACAGAAA; *MMP1* reverse, TTCGGGGAGAA GTGATGTTTC; *MMP3* forward, CAATTCATGAGCAGCAACG; *MMP3* reverse, AGGGATTAATGGAGATGCCCC; *CXCL1* forward, CTTCTCTCT CCCTTCTGGTC; *CXCL1* reverse, GAAAGCTTGCTCAATCCTG; *CXCL10* forward, GCTGATGCAGGTACAGCGT; *CXCL10* reverse, CACCATGAA TCAAACGCGA; *EGFR* forward, AGGCACGAGTAACAAGCTCAC; *EGFR* reverse, ATGAGGACATAACCAGCCACC; *IGF1R* forward, TCGACATCCGCAACGACTATC; *IGF1R* reverse, CCAGGGCGTA GTTGTAGAAGAG; *INSR* forward, AAAACGAGGCCCGAAGATTTC; *INSR* reverse, GAGCCCATAGACCCCGGAAG; *PDGFRB* forward, AGC ACCTTCGTTCTGACCTG; *PDGFRB* reverse, TATTCTCCCGTGTAGCCCA; *GAPDH* forward, AAGGTGAAGGTCGGAGTCAA; *GAPDH* reverse, AATGAAGGGGTCATTGATGG. All reactions were run in triplicate.

Human phospho-receptor tyrosine kinase array. Phospho-receptor tyrosine kinase (RTK) arrays were used to analyse alterations of kinase signalling in response to treatment with AZD8055 in Hep3B cells, according to the manufacturer's instructions (R&D systems).

Xenografts. All mice were manipulated according to protocols approved by the Shanghai Medical Experimental Animal Care Commission and Shanghai Cancer Institute. The maximum permitted tumour volume was 2,000 mm³. Huh7 and MHCC97H cells (5 × 10⁶ cells per mouse) were injected subcutaneously into the right posterior flanks of 6-week-old BALB/c nude mice (male, 6–10 mice per group). Tumour volume, based on calliper measurements, was calculated by the modified ellipsoidal formula: tumour volume = 1/2(length × width²). After tumour establishment, mice were randomly assigned to 6 days per week treatment with vehicle, XL413 (50–100 mg/kg, oral gavage), AZD8055 (10–20 mg/kg, oral gavage) or a combination in which each compound was administered at the same dose and schedule as the single agent. For sorafenib-treatment assay, Huh7 and MHCC97H-pLKO cells (5 × 10⁶ cells per mouse) were injected subcutaneously into the right posterior flanks of 6-week-old BALB/c nude mice (male, 6 per group). Mice were randomly assigned to treatment 6 days per week with vehicle or sorafenib (30 mg/kg, daily gavage). The investigators were not blinded to allocation during experiments and outcome assessment.

Immunocompetent mouse models of HCC. All mouse study protocols were approved by the NKI Animal Welfare Body. Vectors for HDTV1 were prepared using the EndoFree-Maxi Kit (Qiagen) and resuspended in a sterile 0.9% NaCl solution/plasmid mix containing 5 µg of pT3-MYC (Addgene 92046), 5 µg of pX330-p53 (Addgene 59910) or pX330-PTEN (Addgene 59909), and 2.5 µg of CMV-SB13 transposase. A total volume mix corresponding to 10% of body weight was injected via lateral tail vein in 5–7 s into 6–8-week-old female C57Bl/6 mice

(Janvier laboratories). Mice were monitored by weekly MRI after HDTV1. MRI was performed in ParaVision 6.0.1 on a 7T Bruker BioSpec 70/20 USR with a ¹H transmit–receive volume coil. T2-weighted images were acquired under 1–2% isoflurane in air and oxygen flow using a respiratory-gated sequence with TR/TE = 2,500/25 ms, 32 × 24-mm field of view (320 × 240 matrix, resolution of 0.1 mm), 30 × 0.7-mm axial slices and 4 averages. MRI images were analysed with MIPAV ('Medical, Image, Processing, Analysis and Visualization' software) to calculate tumour volume. The investigators were not blinded to allocation during experiments and outcome assessment.

When HCCs were first visible by MRI (14–21 days after HDTV1), tumour-size-matched mice were randomized over the treatment groups: vehicle, XL413, AZD8055, a combination of XL413 and AZD8055, or sorafenib. Mice were dosed 6 days per week with vehicle, XL413 (100 mg/kg, oral gavage), AZD8055 (20 mg/kg, oral gavage), a combination in which XL413 and AZD8055 were administered at the same dose as the single agent, or with sorafenib (30mg/kg, oral gavage). For time-point analysis, mice were killed 14–16 days after the initiation of treatment, and for survival-curve and endpoint analysis, the treatment continued until mice were symptomatic (the tumour reached a total volume of ≥2 cm³).

No toxicity was observed over the monotherapy groups. Seventeen per cent of mice showed therapy-induced adverse events in the XL413 + AZD8055 treatment group and 83% of mice showed a well-tolerated response to treatment.

For quantification of SA-β-gal staining, the sample size was as follows: vehicle-treated, *n* = 41 biologically independent nodules from 7 mice; XL413-treated, *n* = 81 biologically independent nodules from 11 mice; AZD8055-treated, *n* = 26 nodules from 3 mice; and combination-treated, *n* = 101 nodules from 13 mice. For quantification of p16 staining, the sample size was as follows: vehicle-treated, *n* = 23 biologically independent nodules from 3 mice; XL413-treated, *n* = 43 biologically independent nodules from 5 mice; AZD8055-treated, *n* = 37 nodules from 3 mice; and combination-treated, *n* = 59 nodules from 8 mice.

Flow cytometry. Mouse livers were perfused with PBS and then dissociated into single-cell suspension using the Liver Dissociation kit (Miltenyi Biotec) and the gentleMACS Octo Dissociator, following the manufacturer's instructions. The cell suspension was passed through a 100-µm cell strainer (Corning) and then centrifuged at 300g for 10 min at 4°C and washed 3 times in FACS buffer. Samples were incubated with anti-CD16/CD32 antibody (BD Biosciences) for 15 min and then stained with the indicated antibodies (Supplementary Table 2) following standard procedures. Samples were fixed with eBioscience fixation and permeabilization kit (Invitrogen) and Ki67 antibody was used for intracellular staining. The signal was detected by using a four-laser Fortessa flow cytometer (Becton Dickinson). Analyses were carried out using FlowJo software. The gating strategy is provided in Supplementary Information. For macrophages, CD4 and CD8 T cells, the sample size was as follows: vehicle-treated, intermediate time point *n* = 7 mice and endpoint *n* = 8 mice; XL413-treated, intermediate time point *n* = 3 mice and endpoint *n* = 6 mice; AZD8055-treated, intermediate time point *n* = 3 mice and endpoint *n* = 5; and combination-treated, intermediate time point *n* = 6 mice and endpoint *n* = 7 mice. For assessment of Ki67⁺ cells in CD4 and CD8 T cell populations, samples sizes were as follows: vehicle-treated, intermediate time point *n* = 7 mice and endpoint *n* = 8 mice; XL413-treated, intermediate time point *n* = 3 mice and endpoint *n* = 4 mice; AZD8055-treated, intermediate time point *n* = 3 mice and endpoint *n* = 5; and combination-treated, intermediate time point *n* = 6 mice and endpoint *n* = 3 mice.

Reporting summary. Further information on research design is available in the Nature Research Reporting Summary linked to this paper.

Data Availability

Raw and processed data from the next-generation RNA sequencing of samples have been deposited in the NCBI Gene Expression Omnibus (GEO) under accession number GSE121276 and GSE121277. All other data can be found in the Source Data, Supplementary Information or are available from the corresponding authors upon reasonable request.

- Garcia Fortanet, J. et al. Allosteric inhibition of SHP2: identification of a potent, selective, and orally efficacious phosphatase inhibitor. *J. Med. Chem.* **59**, 7773–7782 (2016).
- Evers, B. et al. CRISPR knockout screening outperforms shRNA and CRISPRi in identifying essential genes. *Nat. Biotechnol.* **34**, 631–633 (2016).
- Koelzer, V. H. et al. Digital image analysis improves precision of PD-L1 scoring in cutaneous melanoma. *Histopathology* **73**, 397–406 (2018).
- Subramanian, A. et al. Gene set enrichment analysis: a knowledge-based approach for interpreting genome-wide expression profiles. *Proc. Natl Acad. Sci. USA* **102**, 15545–15550 (2005).
- Peng, T., Golub, T. R. & Sabatini, D. M. The immunosuppressant rapamycin mimics a starvation-like signal distinct from amino acid and glucose deprivation. *Mol. Cell Biol.* **22**, 5575–5584 (2002).
- Olive, P. L. & Banáth, J. P. The comet assay: a method to measure DNA damage in individual cells. *Nat. Protoc.* **1**, 23–29 (2006).

Acknowledgements We thank L. Zender, R. Smits, X. Qiao and L. Li for the kind gift of cell lines. This work was funded by grants from the European Research Council (ERC 787925 to R.B.), the Dutch Cancer Society (KWF 12049/2018-2 to L.A., 6702/2014 to B.B. and H.t.R) through the OncoCode Institute and the Center for Cancer Genomics (CGC: <http://cancer-genomics.nl>), the National Basic Research Program of China (973 Program: 2015CB553905), the National Key Sci-Tech Special Projects of Infectious Diseases of China (2018ZX10732202-002-003), the National Natural Science Foundation of China (81920108025, 81421001, 81672933, and 81874229), Shanghai Municipal Education Commission-Gaofeng Clinical Medicine Grant Support (20181703), Shanghai Municipal Commission of Health and Family Planning (2017YQ064 and 2018YQ20) and Shanghai Rising-Star Program (18QA1403900). We thank the facilities of Netherlands Cancer Institute: Animal Laboratory, Mouse Clinic Imaging Unit, Experimental Animal Pathology, Flow Cytometry, Sequencing and Bioluminescence Imaging.

Author contributions C.W. and R.B. conceived the idea and designed the study. R.B., L.A., W.Q. and R.L.B. supervised all research. R.B., L.A., C.W. and S.V. wrote the manuscript and prepared the figures. C.W. designed, performed and analysed *in vitro* experiments and interpreted the results of the xenograft model. S.V. designed, performed and analysed *in vivo* data conducted on the immunocompetent mouse models with technical support from J.G. H.J. and

D.G. performed xenograft experiments. B.B. designed, performed and analysed neutral comet assays. C.L. and B.E. performed data analysis. C.R. performed quantification analyses of *in vivo* staining. B.M. performed the GPCR-compound screen. W.W. performed immunofluorescence. A.d.C. and A.M.S. performed and analysed SHP2 experiments. G.J. provided clinical samples. R.L.d.O., L.W., Z.X., A.S., F.J., S.M. and H.t.R. provided advice for the project. All authors commented on the manuscript.

Competing interests C.W. and R.B. are listed as inventors of a patent application using the one-two punch therapy (CDC7 inhibitor and mTOR inhibitor) for liver cancers with *TP53* mutations. R.B. is the founder of the company Oncosense, which exploits pro-senescence therapies for cancer.

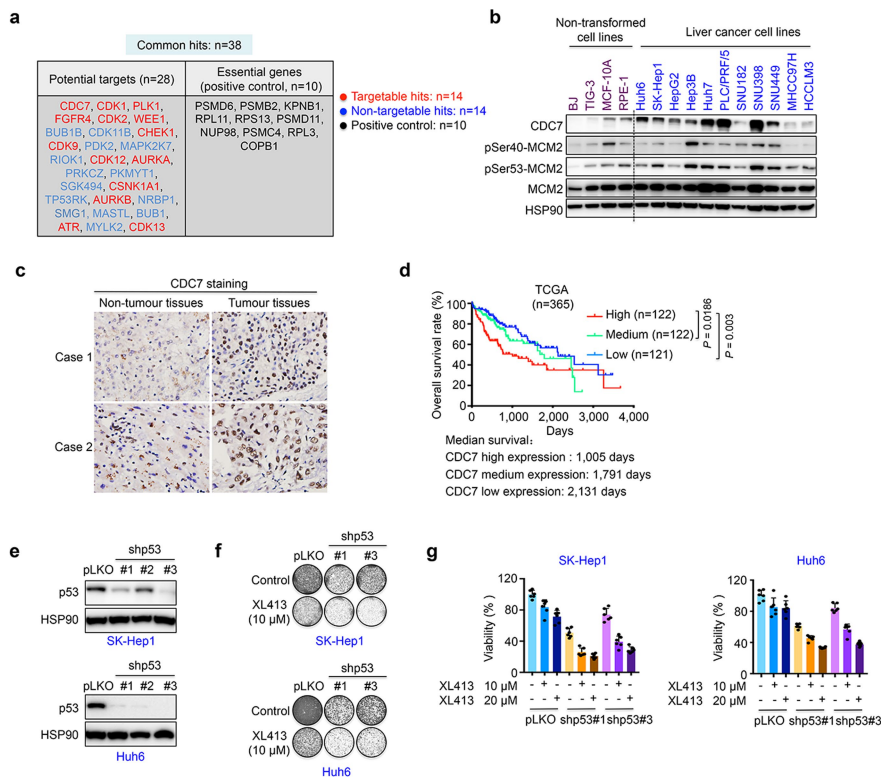
Additional information

Supplementary information is available for this paper at <https://doi.org/10.1038/s41586-019-1607-3>.

Correspondence and requests for materials should be addressed to W.Q., L.A. or R.B.

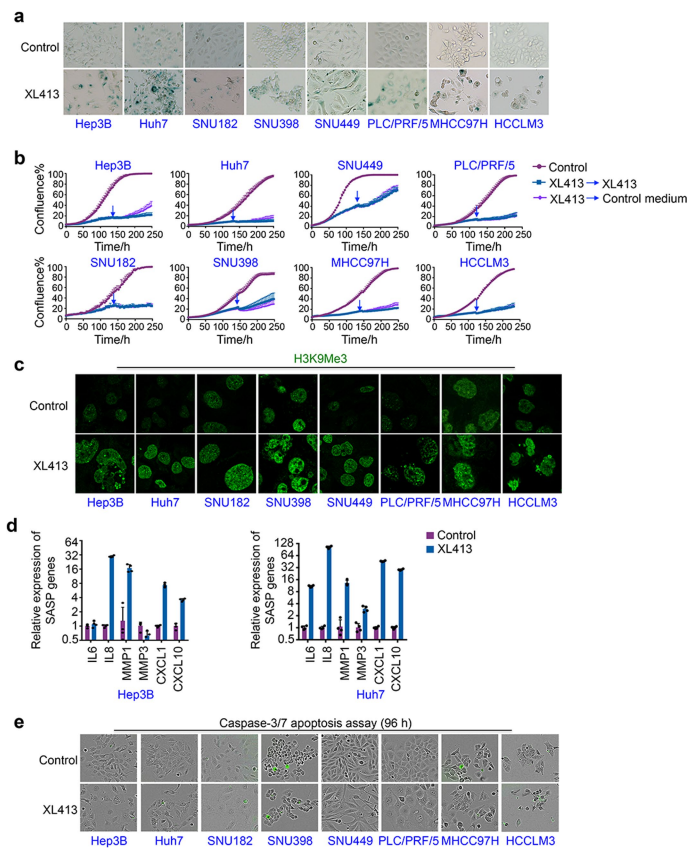
Peer review information *Nature* thanks Hisao Masai and the other, anonymous, reviewer(s) for their contribution to the peer review of this work.

Reprints and permissions information is available at <http://www.nature.com/reprints>.



Extended Data Fig. 1 | Upregulation of *CDC7* mRNA correlates with poor prognosis of patients with HCC, and *TP53* knockdown sensitizes liver cancer cells with wild-type *TP53* to the *CDC7* inhibitor. **a**, Thirty-eight common hits (among the top-50 most-strongly depleted hits in each cell line) were identified by CRISPR screen in Hep3B and Huh7 cells. Hits in red represent factors that are targetable with small-molecule compounds. Blue represents non-targetable hits. **b**, Western blot analysis of levels of *CDC7*, *MCM2* and phosphorylated *MCM2* in non-transformed cell lines and liver cancer cell lines. *HSP90* served as a loading control. **c**, Immunohistochemical analysis showing increased expression of *CDC7* in HCC tissues, compared to paired adjacent non-tumour tissues. **d**, According to the level of *CDC7* mRNA obtained from the TCGA database ($n = 365$ patients), patients with HCC were classified into 3 groups: the top 33.3% were considered as high-expression, the medium 33.3% were considered as intermediate-expression and the lowest 33.3% were considered as low-expression. Kaplan–Meier curves depicting that upregulation of *CDC7* mRNA correlates with poor prognosis of patients with HCC. Statistical significance was calculated using a two-sided

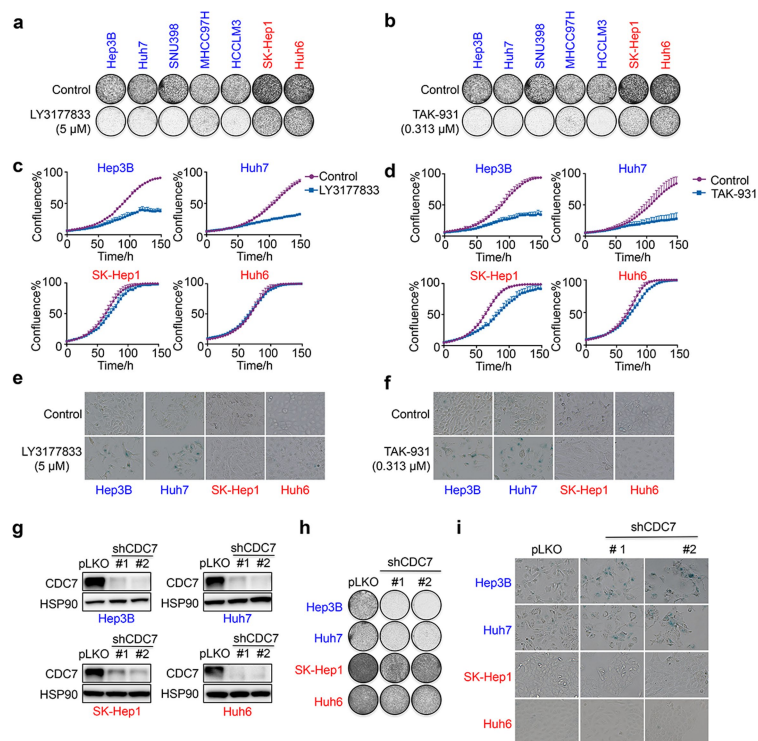
log-rank test. **e**, Liver cancer cell lines with wild-type *TP53* (SK-Hep1 and Huh6) were stably transduced with control pLKO vector or with one of three independent shRNAs that target *TP53* (labelled here as shp53 #1, #2 and #3). On the basis of knockdown efficiency, *TP53* shRNA no. 1 and *TP53* shRNA no. 3 were selected for further experiments. **f**, SK-Hep1 and Huh6 cells that express a control shRNA (pLKO) or knockdown of *TP53* (shp53) were exposed to the indicated concentrations of XL1413 in colony-formation assays. Cells were fixed, stained and photographed after 10–14 days of culture. **g**, SK-Hep1 and Huh6 cells expressing control shRNA or shRNA against *TP53* were exposed to the indicated concentrations of XL1413 for five days. CellTiter-Blue viability assays revealed that *TP53* knockdown synergizes with treatment with XL1413 in SK-Hep1 and Huh6 cells. Graphs represent mean \pm s.d. from six technical replicates. For gel source images, see Supplementary Fig. 1. Data in **a**, **b**, **e–g** are representative of three independent biological experiments. Data in **c** are representative images from immunohistochemical analyses using a tissue microarray containing 80 specimens of HCC.



Extended Data Fig. 2 | Inhibition of CDC7 induces senescence

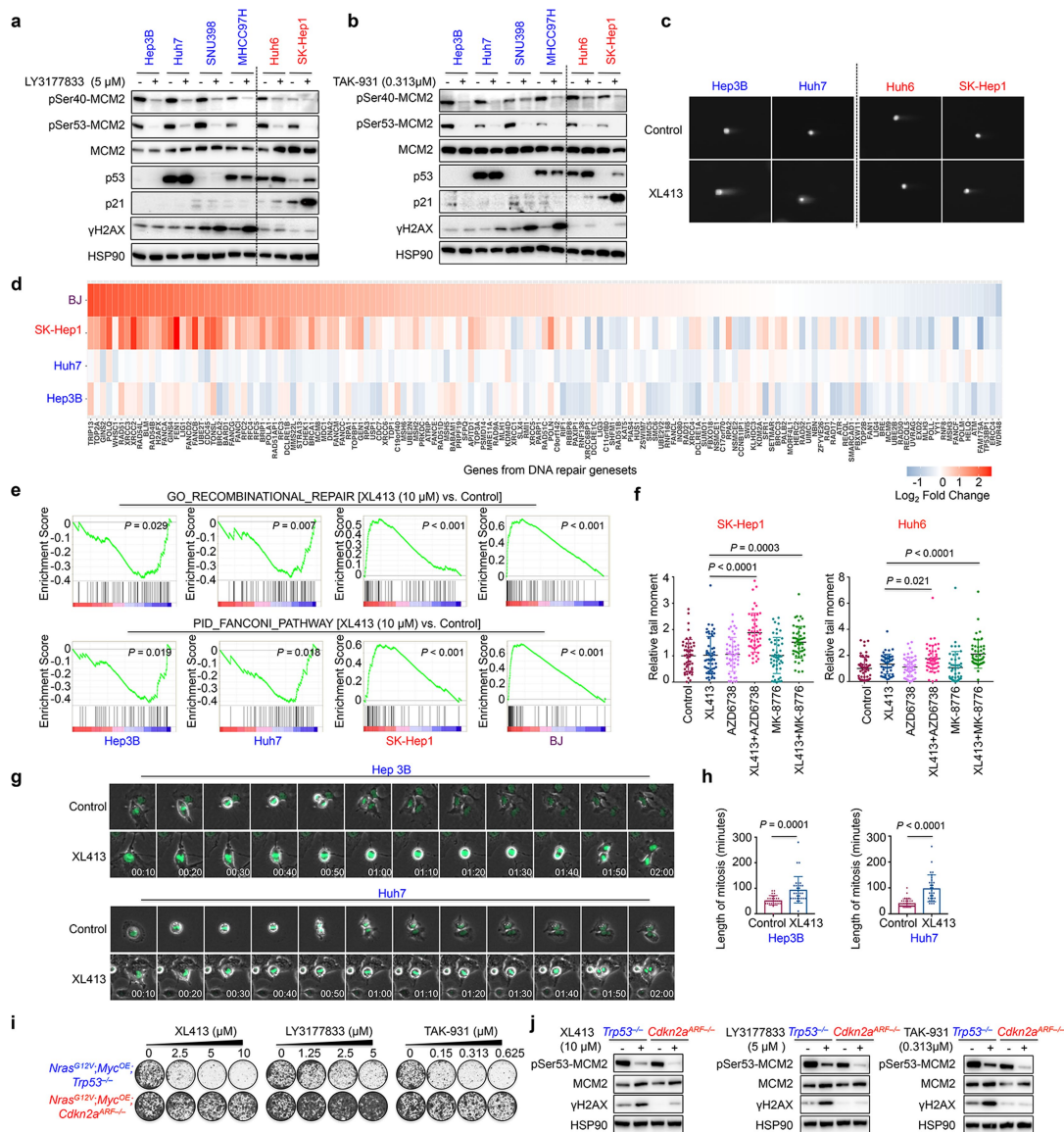
a, Liver cancer cell lines with *TP53* mutation were cultured in the presence of 10 μ M XL413 for 4 days, which induces senescence (as detected by SA- β -gal staining). **b**, Growth curves (measured by Incucyte live-cell analyses) of liver cancer cell lines with *TP53* mutations that were either untreated, continuously treated with XL413 or treated with 10 μ M of XL413 for 5 or 6 days before withdrawal of treatment. Graphs represent mean \pm s.d. from five technical replicates. **c**, Representative images of H3K9me3 staining in liver cancer cell lines with *TP53* mutations, exposed to 10 μ M XL413 for 7 days.

d, Treatment with XL413 induces a senescence-associated secretory phenotype (SASP) in Hep3B and Huh7 cells treated with 10 μ M XL413 for 7 days. mRNA expression of genes associated with the senescence-associated secretory phenotype was determined by qRT-PCR analysis. Graphs represent mean \pm s.d. from four technical replicates. **e**, Liver cancer cells were cultured in the presence of 10 μ M XL413 for 4 days, and apoptotic cells were visualized by caspase-3 and caspase-7 apoptosis assay. Data in **a** are representative of three independent biological experiments. Data in **b–e** are representative of two independent biological experiments.



Extended Data Fig. 3 | Pharmacological or genetic inhibition of CDC7 induces a senescent phenotype in liver cancer cells with TP53 mutations. **a, b,** Liver cancer cell lines with TP53 mutations (Hep3B, Huh7, SNU398, MHCC97H and HCCLM3) (blue) and liver cancer cell lines with wild-type TP53 (SK-Hep1 and Huh6) (red) were seeded at low confluence and grown in the absence or presence of the CDC7 inhibitors LY3177833 or TAK-931 at the indicated concentrations, in long-term colony-formation assays. Cells were fixed, stained and photographed after 10–14 days of culture. **c, d,** Growth curves (measured by Incucyte live-cell analyses) of liver cancer cell lines with TP53 mutations (Hep3B and Huh7) (blue) and liver cancer cell lines with wild-type TP53 (SK-Hep1 and Huh6) (red) exposed to LY3177833 or TAK-931. Graphs represent mean \pm s.d. from four technical replicates. **e, f,** Liver cancer cells were cultured in the presence of the CDC7 inhibitors LY3177833 or TAK-931 at the indicated concentration for 4 days. SA- β -gal staining revealed that CDC7 inhibitors (LY3177833 or TAK-931) selectively induced senescence in liver cancer

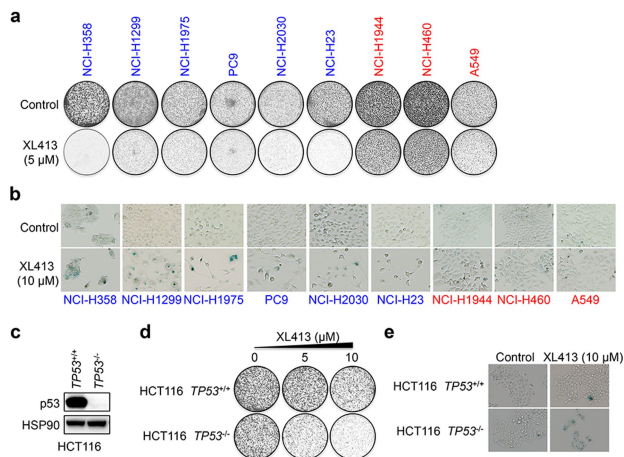
cells with TP53 mutations (blue) and not in liver cancer cells with wild-type TP53 (red). **g,** Liver cancer cell lines with TP53 mutations (Hep3B and Huh7) and liver cancer cell lines with wild-type TP53 (SK-Hep1 and Huh6) were stably transduced with control pLKO vector or with two independent shRNAs that target CDC7 (labelled here shCDC7 #1 and #2) and the efficiency of CDC7 knockdown in liver cancer cell lines was evaluated by western blot. **h,** Colony-formation assays of liver cancer cell lines with TP53 mutation (blue) and liver cancer-cell lines with wild-type TP53 (red), with and without CDC7 knockdown, were performed. Cells were fixed, stained and photographed after ten days of culture. **i,** CDC7 knockdown induced senescence in Hep3B and Huh7 cells with TP53 mutations, but not in SK-Hep1 and Huh6 cells, which have wild-type TP53. Senescence was detected by SA- β -gal staining. For gel source images, see Supplementary Fig. 1. Data in **a–i** are representative of three independent biological experiments.



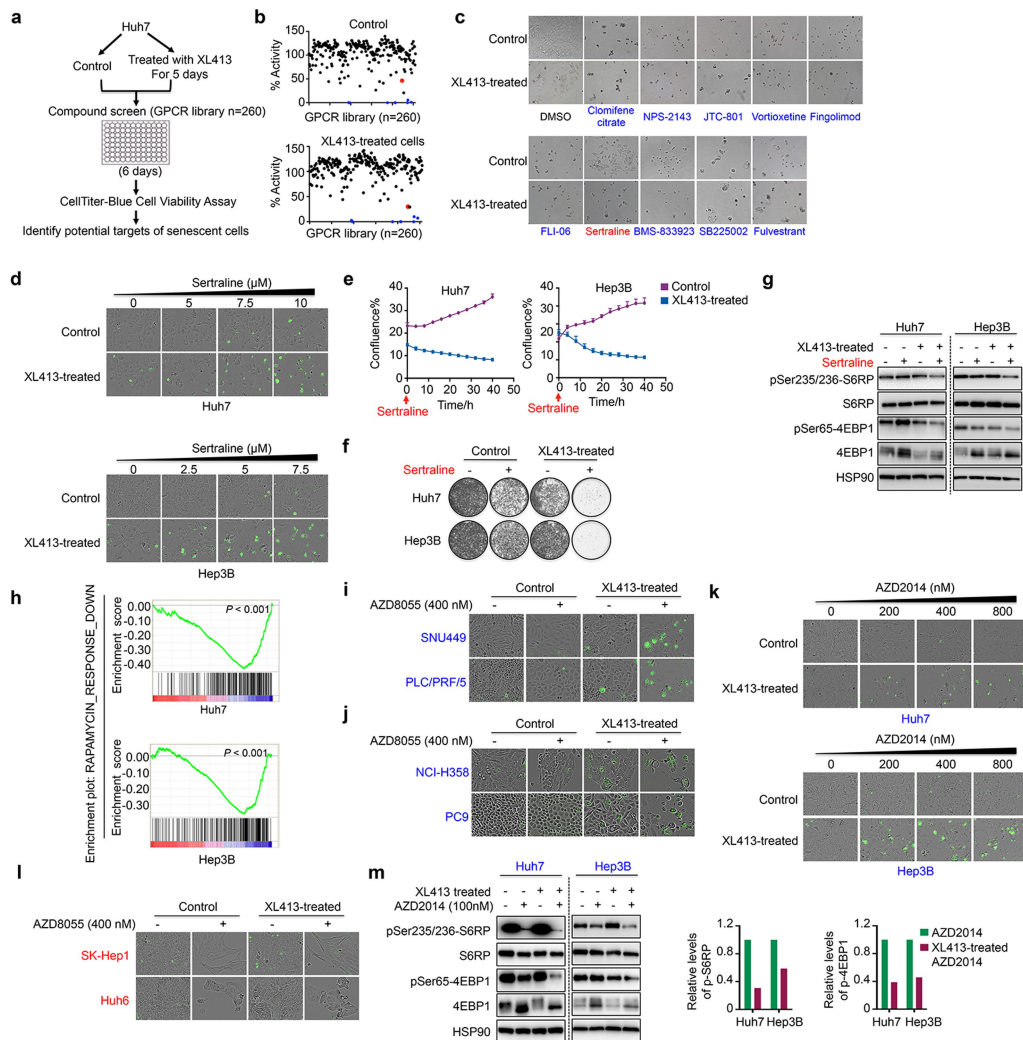
Extended Data Fig. 4 | Inhibition of CDC7 leads to the accumulation of DNA damage specifically in liver cancer cells with TP53 mutations.

a, b, Western blot analysis of liver cancer cell lines treated with CDC7 inhibitors (LY3177833 or TAK-931) for seven days. Inhibition of CDC7 induces the expression of the DNA-damage marker γ H2AX in liver cancer cells with TP53 mutations while lower γ H2AX together with functional upregulation of p53 and p21^{CIP1} were observed in TP53 wild-type liver cancer cell lines post-XL413 treatment. **c**, Representative neutral-comet assay images of liver cancer cells with TP53 mutations (Hep3B and Huh7) and liver cancer cells with wild-type TP53 (SK-Hep1 and Huh6) treated with XL413 for seven days. **d**, Heat map displays fold gene-expression changes (expressed in log₂) in cells with wild-type TP53 (BJ) and SK-Hep1) and liver cancer cells with TP53 mutations (Huh7 and Hep3B) upon treatment with XL413 (10 μ M, 4 days). **e**, GSEA was performed on RNA-sequencing data from Hep3B, Huh7, SK-Hep1 and BJ cells treated with 10 μ M XL413 for 4 days; this identified DNA-repair signatures (recombinational repair and Fanconi anaemia pathway) to be significantly different between cells with TP53 mutations and cells with wild-type TP53 (Methods). **f**, Neutral comet assays were performed on SK-Hep1

and Huh6 cells treated with 20 μ M XL413 combined with AZD6738 (ATR inhibitor, 2.5 μ M) or MK-8776 (CHK1 inhibitor, 2.5 μ M) for 3 days. The value of tail moments in each treatment group were normalized on the basis of the mean value of the control cells ($n = 50$ cells per cell line and condition). Graphs represent mean \pm s.d., analysed with unpaired two-sided Student's *t*-test. **g, h**, H2B-GFP Hep3B and Huh7 cells were cultured in absence or presence of XL413 (10 μ M), and time-lapse microscopy was performed over 96 h to measure the length of mitosis. Graphs represent mean \pm s.d. $n = 30$ cells per cell line and condition, analysed with unpaired two-sided *t*-test. **i**, Mouse cell models of liver cancer with different genetic backgrounds ($Nras^{G12V};Myc^{OE};Tp53^{-/-}$ and $Nras^{G12V};Myc^{OE};Cdkn2a^{ARF-/-}$) were exposed to the indicated concentrations of CDC7 inhibitors (XL413, LY3177833 or TAK-931) for seven days in colony-formation assays. **j**, Western blot analysis of mouse cell models of liver cancer treated with XL413, LY3177833 or TAK-931 for seven days. For gel source images, see Supplementary Fig. 1. Data in **a–c, f, g, h** are representative of two independent biological experiments. Data in **i, j** are representative of three independent biological experiments.

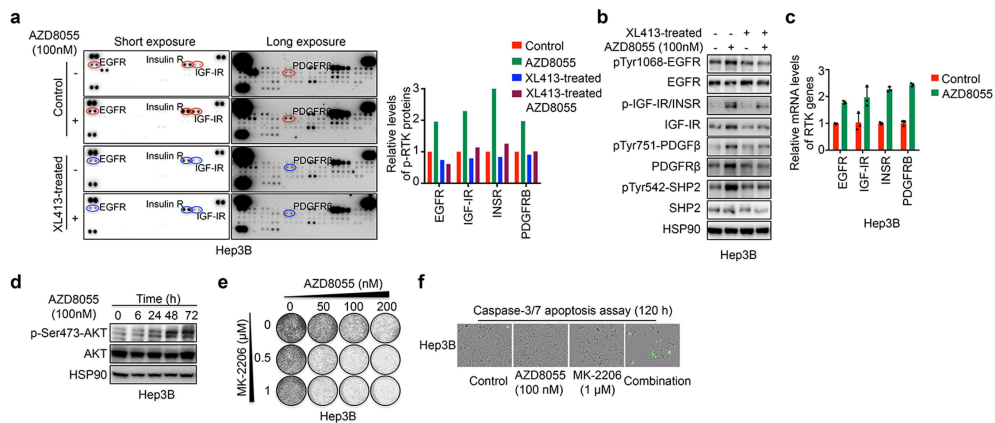


Extended Data Fig. 5 | Inhibition of CDC7 induces senescence selectively in cancer cells with *TP53* mutations. **a**, Lung-cancer cell lines with *TP53* mutations (blue) and lung-cancer cell lines with wild-type *TP53* (red) were seeded at low confluence and grown in the absence or presence of XL413 at the indicated concentration for 10–14 days in colony-formation assays. **b**, Lung-cancer cells were exposed to 10 μ M XL413 for 4 days, which induces senescence selectively in cells with *TP53* mutations (as detected by SA- β -gal staining). **c**, Expression of p53 was assessed in isogenic *TP53*^{-/-} and *TP53*^{+/+} HCT116 colon-cancer cell lines by western blot. **d**, HCT116 *TP53*^{+/+} and HCT116 *TP53*^{-/-} cells were seeded at low confluence and grown in the absence or presence of XL413 at the indicated concentration for seven days in a colony-formation assay, to assess their proliferation capacity. **e**, HCT116 *TP53*^{+/+} and HCT116 *TP53*^{-/-} cells were cultured in the presence of 10 μ M XL413 for 4 days, and senescence was selectively induced in *TP53*^{-/-} HCT116 cells (as detected by SA- β -gal staining). For gel source images, see Supplementary Fig. 1. Data in **a–e** are representative of two independent biological experiments.



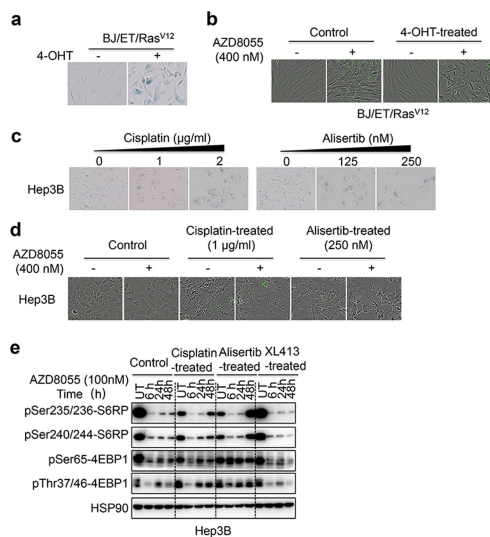
Extended Data Fig. 6 | Sertraline selectively induces apoptosis in XL413-induced senescent cells through the suppression of mTOR signalling. **a**, Schematic of the GPCR-compound screen. Huh7 cells were treated with 10 μ M XL413 for 5 days before seeding in 96-well plates. All compounds were tested at four concentrations for six days, and cell viability was measured using CellTiter-Blue assay. **b, c**, Graph depicting the effects of compounds on cell viability. Each point represents a single compound, with per cent activity calculated by dividing the cell viability score in the presence of 5 μ M of that compound by the mean viability of the negative control. Blue dots indicate compounds that induce cell death in both control and XL413-induced senescent cells. Sertraline (red dot) induced selective cell death in XL413-induced senescent cells. Representative images of the effects of compounds on XL413-treated and untreated cells are shown. **d**, Control cells and XL413-induced senescent cells were sequentially cultured with increasing concentrations of sertraline for 48 h and apoptotic cells were visualized by caspase-3 and caspase-7 apoptosis assay. **e**, Control and XL413-treated cells were sequentially exposed to 10 μ M sertraline, and growth curves were measured by Incucyte live-cell assay. Graphs represent mean \pm s.d. from three technical replicates. **f**, Control and XL413-treated cells were sequentially treated with vehicle or 10 μ M sertraline for 96 h in colony-formation assays. **g**, Control and XL413-treated Huh7 and Hep3B cells were treated with sertraline (10 μ M) for 24 h, and western blot analyses of the indicated proteins of the mTOR signalling pathway were performed. **h**, Hep3B and Huh7 cells were treated with 10 μ M XL413 for 10 days before sequential treatment with sertraline (10 μ M, 24 h), and RNA sequencing was performed. GSEA indicates that the gene set related

to downregulation of mTOR signalling was negatively enriched in liver cancer cells that were sequentially treated with XL413 and sertraline (Methods). **i, j**, Liver cancer cells with *TP53* mutations (SNU449 and PLC/PRF/5) and lung-cancer cell lines with *TP53* mutations (NCI-H358 and PC9) were treated with 10 μ M XL413 or vehicle for 5–7 days, and sequentially exposed to increasing concentrations of AZD8055. Apoptotic cells were visualized by caspase-3 and caspase-7 apoptosis assay 96 h after treatment with AZD8055. **k**, Liver cancer cells with *TP53* mutations (Hep3B and Huh7) were treated with 10 μ M XL413 or vehicle for 7–10 days. Control cells and XL413-induced senescent cells were plated and exposed to increasing concentrations of the mTORC1 and mTORC2 inhibitor AZD2014. Apoptotic cells were visualized by caspase-3 and caspase-7 apoptosis assay 96 h after treatment with AZD2014. **l**, Liver cancer cell lines with wild-type *TP53* (SK-Hep1 and Huh6) were treated with 10 μ M XL413 or vehicle for 5–7 days before exposure to increasing concentrations of AZD8055. Apoptotic cells were visualized by caspase-3 and caspase-7 apoptosis assay 96 h after treatment with AZD8055. **m**, Control cells and XL413-induced senescent cells were treated with AZD2014 for 48 h. Western blot analysis was performed with the indicated antibodies (left) and the levels of phosphorylated S6RP and phosphorylated 4EBP1 were normalized to the total levels of S6RP and 4EBP1, respectively (right); this shows that treatment with AZD2014 leads to strong inhibition of mTOR signalling in XL413-induced senescent cells. For gel source images, see Supplementary Fig. 1. Data in **a–f** are representative of three independent biological experiments. Data in **h–m** are representative of two independent biological experiments.

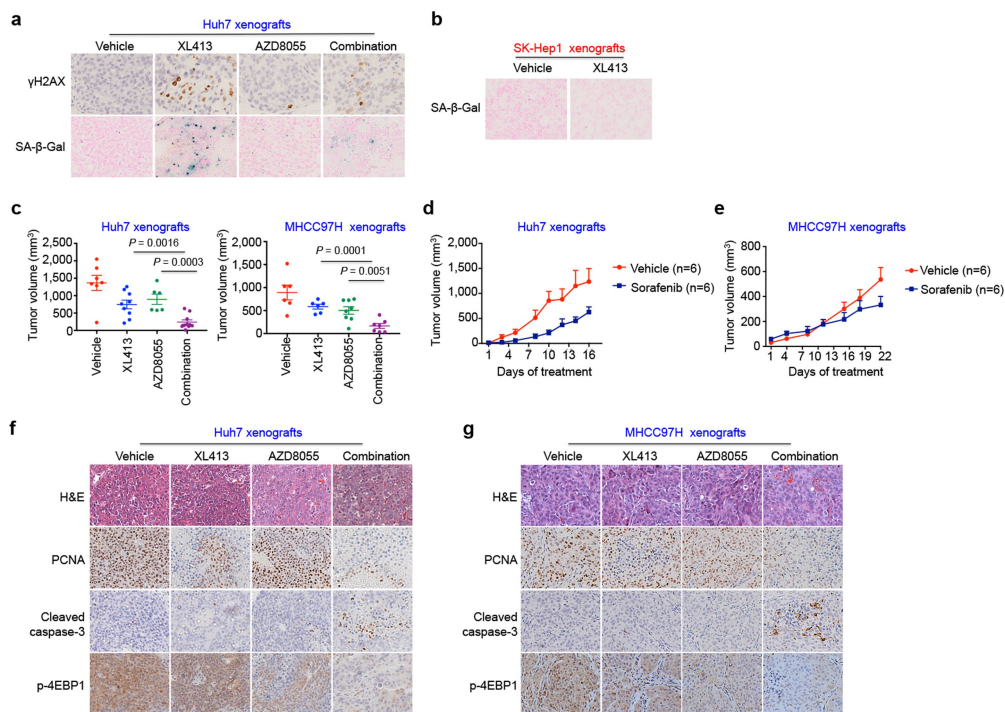


Extended Data Fig. 7 | The activation of RTK feedback that is induced after treatment with AZD8055 is disrupted in XL413-induced senescent cells. **a**, Control cells and XL413-treated Hep3B cells were treated with AZD8055 for 48 h, and extracted proteins were analysed using a human phosphorylated-RTK array kit (left). The levels of phosphorylated RTK proteins were normalized to positive controls (right). **b**, The activation of RTKs identified by RTK arrays and the phosphorylation of SHP2 were validated by western blot analyses. **c**, Hep3B cells were treated with AZD8055 for 48 h before extraction of mRNA, and quantification of the indicated genes for RTK proteins was performed by qRT-PCR. Graph represents mean \pm s.d. from three technical replicates. **d**, Hep3B

cells were treated with AZD8055, and cell lysates were collected at the indicated time points to perform western blot analyses with the indicated antibodies. **e**, Hep3B cells were exposed to increasing concentrations of the AKT inhibitor MK-2206 in combination with AZD8055, and long-term colony-formation assays were performed; this revealed the synergistic effects of these two compounds on cell viability. **f**, Hep3B cells were treated with AZD8055, MK-2206 or a combination of both compounds at the indicated concentrations for five days, and apoptotic cells were visualized by caspase-3 and caspase-7 apoptosis assay. For gel source images, see Supplementary Fig. 1. All experiments shown (except for the RTK array analyses) are representative of two independent biological experiments.

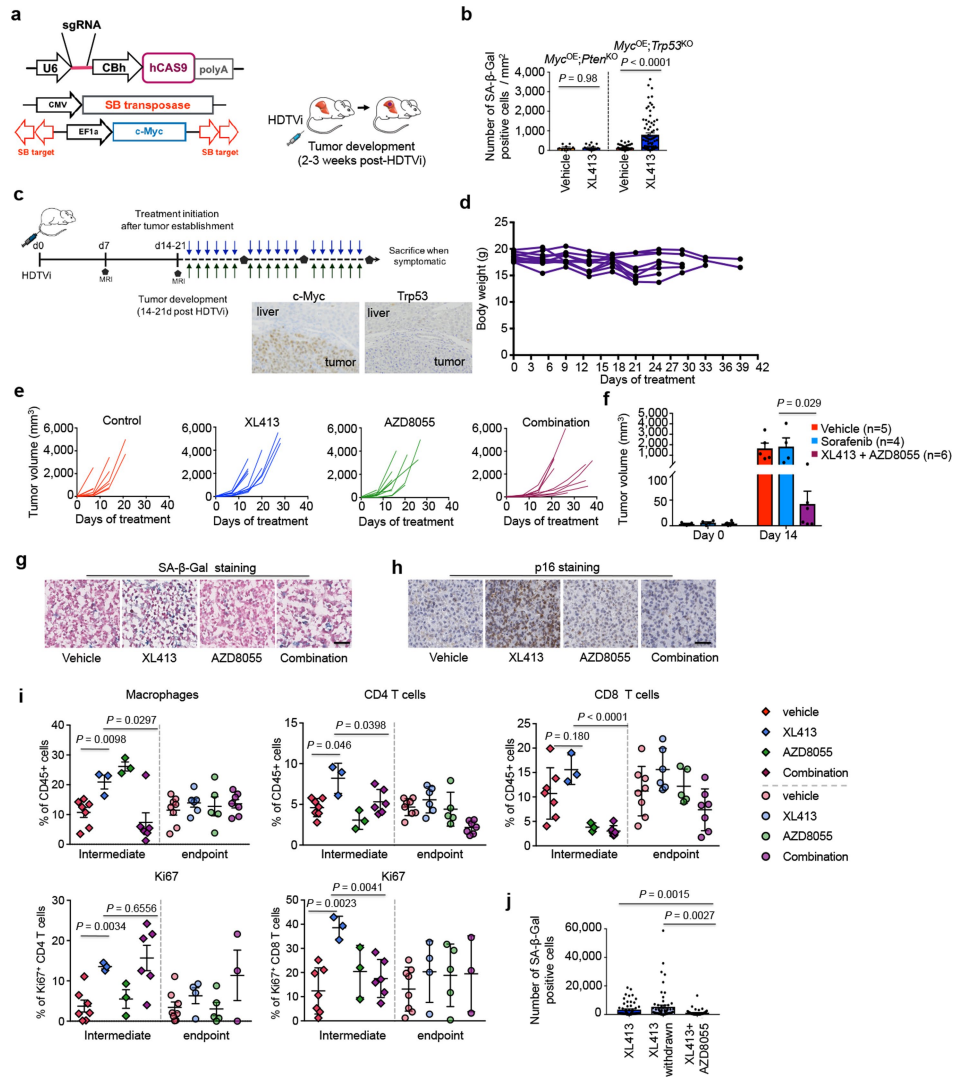


Extended Data Fig. 8 | Treatment with AZD8055 does not induce apoptosis in cisplatin- or alisertib-induced senescent cells. **a**, BJ/ET/RAS^{V12} cells were treated with 100 nM 4-OHT for 21 days to induce senescence, as detected by SA- β -gal staining. **b**, Control or senescent BJ/ET/RAS^{V12} cells were treated either with vehicle or with 400 nM AZD8055 for 96 h, and apoptotic cells were visualized by caspase-3 and caspase-7 apoptosis assay. **c**, Hep3B cells were cultured in the presence of cisplatin or alisertib (aurora-A kinase inhibitor) for 4 days at the indicated concentrations, and the induction of senescence was detected by SA- β -gal staining. **d**, Hep3B cells were treated with cisplatin ($1 \mu\text{g ml}^{-1}$) or alisertib (250 nM) for 4 days, and subsequently exposed to vehicle or 400 nM AZD8055 for 96 h. Apoptotic cells were visualized by caspase-3 and caspase-7 apoptosis assay. **e**, Control cells, or cisplatin-, alisertib- or XL413-induced senescent cells were treated with AZD8055, and cell lysates were collected at the indicated time points. Western blot analyses were performed with the indicated antibodies, which revealed that the mTOR signalling feedback loop is functional in cisplatin- and alisertib-induced senescent cells (whereas it is efficiently inhibited in XL413-induced senescent cells). For gel source images, see Supplementary Fig. 1. Data in **a–e** are representative of two independent biological experiments.



Extended Data Fig. 9 | Pro-senescence treatment combined with an mTOR inhibitor suppresses tumour growth in liver cancer xenografts. **a**, Representative images of γ H2AX and SA- β -gal staining performed on formalin-fixed, paraffin-embedded or frozen sections from subcutaneous Huh7-tumour xenografts treated with vehicle, XL413, AZD8055 or combination of both for 12 days. **b**, Representative images of SA- β -gal staining performed on frozen sections from subcutaneous SK-Hep1-tumour xenografts treated either with vehicle or with XL413 for 21 days. **c**, Tumour-volume measurements in mice bearing Huh7- and MHCC97H-tumour xenografts, treated with vehicle, XL413, AZD8055 or a combination of both, at endpoint (12 days for Huh7 and 22 days for MHCC97H). For sample sizes, see Fig. 4a. One mouse in the vehicle group and one mouse in the XL413 group were excluded from the

analysis, because the maximum permitted tumour volumes (2,000 mm³) were reached in these mice before the endpoint of the trial. Graph shows mean \pm s.e.m., analysed with two-sided unpaired Student's *t*-test. **d**, **e**, Longitudinal progression of tumour volume in mice bearing Huh7 and MHCC97H tumours, treated with vehicle or sorafenib for 16 or 22 days; this revealed that sorafenib therapy has limited efficacy in these two xenograft models. Graph shows mean \pm s.e.m. **f**, **g**, Representative images of haematoxylin and eosin (H & E), PCNA, cleaved caspase-3 and phosphorylated 4EBP1 staining performed on formalin-fixed, paraffin-embedded Huh7 and MHCC97H xenografts from mice killed after the last dose of vehicle, XL413, AZD8055 or a combination of both drugs. Data in **a**, **b**, **f**, **g** are representative of three independent biological experiments.



Extended Data Fig. 10 | See next page for caption.

Extended Data Fig. 10 | Pro-senescence treatment combined with an mTOR inhibitor suppresses tumour growth in p53-deficient, immunocompetent somatic mouse models of HCC. **a**, Schematic of hydrodynamic-tail-vein gene delivery of the *Myc* proto-oncogene transposon system and a CRISPR-Cas9 vector targeting either *Trp53* or the *Pten* tumour suppressor, used to induce models of HCC two to three weeks after HDTV_i. **b**, Quantification of SA- β -gal staining performed on frozen sections from mouse models of *Myc*^{OE};*Pten*^{KO} or *Myc*^{OE};*Trp53*^{KO} HCC, 14 days after treatment with vehicle or XL413 monotherapy (results from *Myc*^{OE};*Trp53*^{KO} HCC are also shown in Fig. 4f). For analyses of *Myc*^{OE};*Pten*^{KO} tumours, vehicle-treated, $n = 9$ biologically independent nodules from 3 mice; XL413-treated, $n = 16$ biologically independent nodules from 3 mice. For analyses of *Myc*^{OE};*Trp53*^{KO} tumours, vehicle-treated, $n = 41$ biologically independent nodules from 7 mice; XL413-treated, $n = 81$ biologically independent nodules from 11 mice. Graph shows the mean \pm s.e.m. of the number of SA- β -gal⁺ cells per tumour nodule per mm². Statistics were calculated by two-sided unpaired Student's *t*-test. **c**, Trial design to evaluate the efficacy of the pro-senescence treatment combined with an mTOR inhibitor in mice bearing *Myc*^{OE};*Trp53*^{KO} HCC. Mice were monitored by weekly MRI after HDTV_i, and enrolled into treatments with vehicle, XL413 (100 mg kg⁻¹, daily gavage), AZD8055 (20 mg kg⁻¹, daily gavage) or XL413 + AZD8055 combination at the first signs of tumour development (revealed by MRI). Drugs were administered six days per week, and mice were killed when they became symptomatic. Immunohistochemical analyses confirmed MYC expression and p53 knockout in endpoint *Myc*^{OE};*Trp53*^{KO} HCC. **d**, Longitudinal individual-body-weight curves from mice bearing *Myc*^{OE};*Trp53*^{KO} tumours, treated with the combination of XL413 + AZD8055. **e**, Individual tumour-growth curves from mice treated with vehicle, XL413, AZD8055 or a combination of both drugs were calculated on the basis of MRI images from mice bearing *Myc*^{OE};*Trp53*^{KO} tumours. **f**, Volumes of *Myc*^{OE};*Trp53*^{KO} tumours from mice

bearing HCC, treated with vehicle ($n = 5$, as shown in Fig. 4c), sorafenib ($n = 4$) or XL413 + AZD8055 ($n = 6$) at day 0 and day 14. Graphs show mean \pm s.e.m., analysed with two-sided unpaired Student's *t*-test. **g**, **h**, Representative images of SA- β -gal (**g**) and p16 (**h**) staining performed on frozen and paraffin-embedded sections, respectively, from mice bearing *Myc*^{OE};*Trp53*^{KO} tumours, treated with the indicated drugs and killed at the intermediate time point (14–16 days in time-matched treated cohorts). Quantifications are shown in Fig. 4f, g. Scale bar, 50 μ m. **i**, Mice bearing *Myc*^{OE};*Trp53*^{KO} tumours, treated with vehicle, XL413, AZD8055 or a combination of both drugs were killed at the indicated time point after treatment. Tumours were dissociated as single-cell suspensions, and flow cytometry analyses were performed to determine the content of tumour-associated macrophages (CD45⁺ CD11b⁺ Ly6C⁻ Ly6G⁻), CD8 T cells (CD45⁺ CD3⁺ CD19⁻ NK1.1⁻ CD8⁺) and CD4 T cells (CD45⁺ CD3⁺ CD19⁻ NK1.1⁻ CD4⁺) relative to total CD45⁺ leucocytes. Cell proliferation (Ki67⁺) was determined within CD8 T cells and CD4 T cell populations. Graphs show mean \pm s.e.m., analysed with two-sided unpaired Student's *t*-test. Sample sizes are given in Methods. **j**, Mice bearing *Myc*^{OE};*Trp53*^{KO} HCC were treated with XL413 ($n = 20$) or XL413 + AZD8055 combination ($n = 8$) for 14 days. Among the XL413-treated mice, a subset ($n = 10$) was killed at 14 days after treatment, concomitantly with the group treated with the combination of drugs. The rest of the XL413-treated mice ($n = 10$) underwent withdrawal of XL413 for 4 days. The absolute number of senescent cells per tumour nodule were visualized by SA- β -gal staining, performed on frozen sections and quantified for each treatment group (XL413-treated, $n = 60$ biologically independent nodules from 10 mice; XL413-withdrawn, $n = 63$ biologically independent nodules from 10 mice; XL413 + AZD8055-treated, $n = 57$ biologically independent nodules from 7 mice). Graphs show mean \pm s.e.m. analysed with two-sided unpaired Student's *t*-test. Data in **c** are representative of three independent biological experiments.